Fracture Mechanics of Concrete Structures
Proceedings FRAMCOS-3
AEDIFICATIO Publishers, D-79104 Freiburg, Germany

CONTRIBUTION OF A CONCRETE COMPACTION MODEL TO AN IMPACT PROBLEM

F. Gatuingt, N. Burlion, and L. Daudeville
Division of Civil Engineering & Environment, LMT-Cachan, ENS Cachan / CNRS and Research Network GEO, France
G. Pijaudier-Cabot
Division of Civil Engineering & Environment, LMT-Cachan, ENS Cachan / CNRS and Institut Universitaire de France, France
T. Bouet
TDA Armements SAS, La Ferte St Aubin, France

Abstract
In the analysis of structures subjected to blasting or impacts, concrete experiences compaction, a decrease of porosity, plastic strains in compression and also cracking in tension. The objective of this study is to develop a constitutive model for concrete which covers this entire range of material nonlinearity. Hence a coupled damage and plasticity constitutive model for concrete under fast dynamic loading is developed. This model is based on mechanics of porous materials, damage and plasticity. The constitutive relations are presented and compared with experimental results. The computational implementation has been carried out in the Lagrangian finite element code DYNA3D. In order to show the influence of compaction, simulations of a split Hopkinson test performed on confined concrete and a concrete slab subjected to an impact have been carried out. Comparisons between simulations with a classical plasticity model and the present model are discussed in order to exhibit the influence of concrete compaction.
Key words: Compaction, Damage mechanics, Plasticity, Porous materials

1 Introduction

In a concrete structure subjected to a shock or to an impact, the material experiences severe hydrostatic stresses and compaction. Then, propagation and reflection of waves produce eventually tensile cracking and spalling. Tensile cracking is, however, controlled by the compressive response of the material and it is important to describe the compressive phase of the material response as accurate as possible in order to predict failure. A phenomenological model based on continuum damage mechanics combined with plasticity is presented for this purpose.

In tension, the proposed model is based on a classical scalar damage model. In the case of compaction of concrete, it is important to take into account both the growth in plastic strains and the decrease in porosity which results in an increase in the elastic stiffness of the material. In order to describe this type of material response, the plasticity model coupled with the damage model is implemented. We have used a modified Gurson's yield function for this purpose with associated flow rules (Gurson 1977, Needleman and Tvergaard 1984). The evolution of the volume fraction of voids is directly related to the irreversible variation of volume fraction of material. When it decreases, it produces an increase in the material stiffness and therefore a decrease in damage which is not common in the conventional damage models.

Experimental results have shown that it is not possible to separate the deviatoric and hydrostatic responses of the material as in usual models for impact problems (Burlion, 1997). This phenomenon is well captured by the model. Numerical simulations which exhibit the influence of compaction and comparisons with an elastic plastic model are presented on an impact problem.

2 Compaction of concrete : a coupled damage and plasticity model

Let us first recall the constitutive relations in the tensile regime: we use here a scalar damage model. Within the classical framework of (small strain) elasto-plasticity, we use the basic assumption of additive strain decomposition:

$$d\varepsilon_{ij}(x,t) = d\varepsilon_{ij}^{rev}(x,t) + d\varepsilon_{ij}^{irr}(x,t) \qquad (2.1)$$

where $\varepsilon_{ij}(x,t)$ are the total strain components, $\varepsilon_{ij}^{irr}(x,t)$ are the irreversible strain components and $\varepsilon_{ij}^{rev}(x,t)$ are the reversible strain components.

The stress-strain relation is, in the absence of plastic strain growth:

$$\sigma_{ij} = (1-d)\left[\lambda \varepsilon_{kk}^{rev} \delta_{ij} + 2\mu \varepsilon_{ij}^{rev}\right] \tag{2.2}$$

where λ and μ are the Lamé coefficients. d is the scalar damage variable. In the tensile regime, and as we will see further more generally in the absence of plastic strain growth, we use the evolution laws for damage proposed by Mazars (1986).

Hydrostatic compression produces a collapse of the microstructure and a decrease in porosity. In these situations, concrete exhibits elastic-plastic behaviour with an increase of the elastic stiffness upon unloading. In order to take into account this phenomenon in the model, we have chosen to describe the compressive regime with a plasticity model where the damage variation is also coupled to the plastic strains in order to capture the material elastic stiffening.

Micromechanical modelling of the effect of micro-voids on the plastic behaviour has been done by Gurson for elastic perfectly-plastic alloys containing spherical voids (Gurson, 1977). A modified version of this model is chosen here for the plastic part (Needleman and Tvergaard, 1984). The yield function is defined by:

$$F_{NT}(\sigma_{ij}, \sigma_M, f^*) = \frac{3J_2}{\sigma_M^2} + 2q_1 f^* \cosh\left(q_2 \frac{I_1}{2\sigma_M}\right) - (1 + (q_3 f^*)^2) = 0 \tag{2.3}$$

where I_1 is the first stress tensor invariant and J_2 is the second invariant of the deviatoric stress tensor.

$$I_1 = \sigma_{kk}\delta_{ij} \qquad J_2 = \frac{1}{2}(s_{ij}s_{ij}) \qquad s_{ij} = \sigma_{ij} - \frac{1}{3}\sigma_{kk}\delta_{ij} \tag{2.4}$$

σ_M is the equivalent yield stress in the matrix, f^* is the volume fraction of voids. f^* increases with void development in tension, and decreases with void closure in triaxial compression. $q_1, q_2,$ and q_3 are model parameters.

The evolution of the modified Gurson's yield surface with the decrease in porosity is presented in Fig. 1. Note that the yield surface is only plotted in a quarter quadrant of the $(J_1/\sigma_M, \sqrt{3J_2}/\sigma_M)$ space. The yield surface grows due to the closure of the material porosity (or decrease in the volume fraction of voids). Finally, it must be underlined that when the

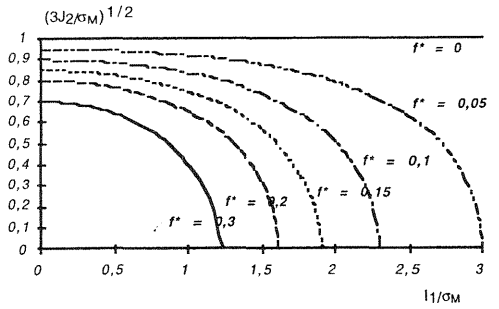

Fig. 1. Modified Gurson yield function : evolution with the decrease of porosity ($q_1 = q_2 = q_3 = 1$).

volume fraction of voids is equal to zero the loading function reduces to the classical Von Mises expression.

A dissipated energy equivalence defines equivalent strain (ε_M) and stress (σ_M) in the matrix:

$$\sigma_{ij} d\varepsilon_{ij}^{irr} = (1 - f^*)\sigma_M d\varepsilon_M^{irr} \quad (2.5)$$

The relation between ε_M and σ_M is defined through a simple elastic-plastic model with non-linear hardening.

The volume fraction evolution is assumed to be controlled by the irreversible strain increment:

$$df^* = (1 - f^*) f^* d\varepsilon_{kk}^{irr} \quad (2.6)$$

The plastic flow is associated and the normality rule gives the following expressions for the irreversible strain increments:

$$\begin{cases} d\varepsilon_{ij}^{irr} = d\lambda \dfrac{\partial F_{NT}}{\partial \sigma_{ij}} \\ d\varepsilon_M^{irr} = -d\lambda \dfrac{\partial F_{NT}}{\partial \sigma_M} \end{cases} \quad (2.7)$$

where ε_M^{irr} is the irreversible strain in the matrix associated with σ_M, and the plastic multiplier $d\lambda$ is defined according to the consistency condition. Finally, damage due to both tensile cracking and compaction is written in an additive fashion:

$$d = g(\tilde{\varepsilon}) + f^* \quad (2.8)$$

where $g(\tilde{\varepsilon})$ is the evolution of damage in the model by Mazars in the absence of compression.

3 Numerical implementation

The present constitutive relation has been implemented in the commercial finite element code DYNA3D. It is a vectorised explicit three-dimensional finite element code for analysing the large deformation dynamic response of inelastic solids. In this code the equations of motion are integrated in a time domain with the explicit central difference method.

The implementation of the model consists in computing the stress vector at each time step. Because of the explicit time integration of the equations of motion, we are going to derive the explicit form of the stress increment as a function of the total strain increment under the assumption that damage and plastic strains evolve simultaneously. Within a predictor-corrector scheme, the loading function of damage is tested first assuming that there is no plastic strain. Then, the loading function for the plastic part is tested according to the predictor and a plastic correction is computed. Tensile damage is tested first because if there is no plasticity, the tensile strains will be in most cases the largest possible ones. Nevertheless, the damage loading function is rechecked when the elastic strains have been determined according to the plastic model. Eq. (2.3) gives by differentiation:

$$dF_{NT}(\sigma_{ij},\sigma_M,f^*) = \frac{\partial F_{NT}}{\partial \sigma_{ij}} d\sigma_{ij} + \frac{\partial F_{NT}}{\partial \sigma_M} d\sigma_M + \frac{\partial F_{NT}}{\partial f^*} df^* = 0 \tag{3.1}$$

with:

$$\begin{cases} \dfrac{\partial F_{NT}}{\partial \sigma_{ij}} = \dfrac{3}{\sigma_M^2} s_{ij} + \dfrac{q_1 q_2 f^*}{\sigma_M} \left[\sinh\left(\dfrac{q_2 I_1}{2\sigma_M}\right) \right] \delta_{ij} \\ \dfrac{\partial F_{NT}}{\partial \sigma_M} = -2\dfrac{J_2}{\sigma_M^3} - \dfrac{q_1 q_2 f^* I_1}{\sigma_M^2} \left[\sinh\left(\dfrac{q_2 I_1}{2\sigma_M}\right) \right] \\ \dfrac{\partial F_{NT}}{\partial f^*} = 2q_1 \left[\cosh\left(\dfrac{q_2 I_1}{2\sigma_M}\right) \right] - 2q_3 f^* \end{cases} \tag{3.2}$$

These partial derivatives are known at each time step and it is possible to write Eq. (3.1) explicitly as follows:

$$dF_{NT}=\frac{3}{\sigma_M^2}s_{ij}d\sigma_{ij}+\frac{q_1q_2f^*}{\sigma_M}\left[\sinh\left(\frac{q_2I_1}{2\sigma_M}\right)\right]\delta_{ij}d\sigma_{ij}-\left[2\frac{J_2}{\sigma_M^3}+\frac{q_1q_2f^*I_1}{\sigma_M^2}\left[\sinh\left(\frac{q_2I_1}{2\sigma_M}\right)\right]\right]d\sigma_M \qquad (3.3)$$

$$+2q_1\left[\cosh\left(\frac{q_2I_1}{2\sigma_M}\right)\right]df^*-2q_3f^*df^*=0$$

The evolution of porosity is given by :

$$df^*=d\lambda(1-f^*)f^*\frac{\partial F_{NT}}{\partial\sigma_{ij}}\delta_{ij} \qquad (3.4)$$

and the constitutive relation between the stress and strain increments in the matrix is:

$$d\sigma_M=E_t d\varepsilon_M,\quad \frac{1}{E_t}=\frac{\partial\left[\frac{\sigma_y}{E}\left(\frac{\sigma_M}{\sigma_y}\right)^n\right]}{\partial\sigma_M}=\frac{n}{E}\left(\frac{\sigma_M}{\sigma_y}\right)^{n-1}$$

$$\text{and}\quad d\varepsilon_M^{irr}=\left(\frac{n}{E}\left(\frac{\sigma_M}{\sigma_y}\right)^{1-n}-\frac{1}{E}\right)d\sigma_M=\frac{1}{E^*}d\sigma_M \qquad (3.5)$$

The dissipated energy equivalence (2.5) gives:

$$d\lambda\sigma_{ij}\frac{\partial F_{NT}}{\partial\sigma_{ij}}=(1-f^*)\sigma_M\frac{1}{E^*}d\sigma_M, \qquad (3.6)$$

Hence, the equivalent stress evolution is:

$$d\sigma_M=d\lambda\frac{\sigma_{ij}\frac{\partial F_{NT}}{\partial\sigma_{ij}}E^*}{(1-f^*)\sigma_M} \qquad (3.7)$$

and Eq. (3.3) becomes:

$$\left[\frac{3}{\sigma_M^2}s_{ij}+\frac{q_1q_2f^*}{\sigma_M}\left[\sinh\left(\frac{q_2I_1}{2\sigma_M}\right)\right]\delta_{ij}\right]d\sigma_{ij}-$$

$$\left[2\frac{J_2}{\sigma_M^3}+\frac{qq_2f^*I_1}{\sigma_M^2}\left[\sinh\left(\frac{q_2I_1}{2\sigma_M}\right)\right]\right]d\lambda\frac{\sigma_{ij}\frac{\partial F_{NT}}{\partial\sigma_{ij}}E^*}{(1-f^*)\sigma_M}+ \qquad (3.8)$$

$$\left[2q_1\left[\cosh\left(\frac{q_2I_1}{2\sigma_M}\right)\right]-2q_3f^*\right]d\lambda(1-f^*)f^*\frac{\partial F_{NT}}{\partial\sigma_{ij}}\delta_{ij}=0$$

The increment of the plastic multiplier evolution is derived from the previous equation as a direct function of the stress increment:

$$d\lambda = fct(d\sigma_{ij}) \tag{3.9}$$

The constitutive relation in elasticity is:

$$d\sigma_{ij} = (1-d)C_{ijkl}(d\varepsilon_{ij} - d\lambda\frac{\partial F_{NT}}{\partial \sigma_{ij}}) - ddC_{ijkl}\varepsilon_{kl}^{rev} \tag{3.10}$$

with the help of the evolution law for damage Eq. (2.8), we obtain:

$$\begin{aligned} d\sigma_{ij} &= (1-d)C_{ijkl}(d\varepsilon_{ij} - d\lambda\frac{\partial F_{NT}}{\partial \sigma_{ij}}) - \\ &(\frac{\partial g(\tilde{\varepsilon})}{\partial \tilde{\varepsilon}}\frac{\partial \tilde{\varepsilon}}{\partial \varepsilon_{ij}^{rev}}(d\varepsilon_{ij} - d\lambda\frac{\partial F_{NT}}{\partial \sigma_{ij}}) \\ &+ d\lambda(1-f^*)f^* d\frac{\partial f^*}{\partial \sigma_{ij}}\delta_{ij})C_{ijkl}\varepsilon_{kl}^{rev} \end{aligned} \tag{3.11}$$

Eq. (3.11) combined with Eq. (3.9) provides an explicit expression of the stress increment as a function of the strain increment and under the assumption that both damage due to the tensile reversible strains and plastic strain evolve.

4 Numerical simulation

Two types of computations are going to be presented in the following. The first one is a simulation of the split Hopkinson test aimed at demonstrating the influence of the variation of porosity and inherent stiffening on wave propagation.

In the split Hopkinson test, the input bar is impacted by a striker with an initial velocity which is an experimental parameter. In the input bar a stress wave is developed. This wave arrives at the specimen and becomes the specimen loading. In the output bar, new waves are developed (Fig. 2).

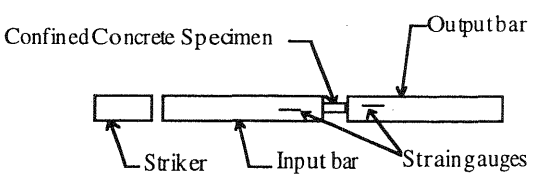

Fig. 2. Split Hopkinson test.

The experimental data are obtained by measuring the strains in the input and output bars. With these strains, we can obtain the experimental velocities and forces (along the cylinder axis) applied on the two faces of the concrete specimen in contact with bars. In order to show the influence of confinement, a special specimen has been designed, made of a concrete cylinder embedded in a metal jacket. The metal jacket controls the radial deformation of the specimen and therefore applies a confinement stress to concrete which avoids splitting. The friction between the concrete sample and the metal jacket has been neglected because, experimentally, the contact surface is coated with Teflon.

In order to show the influence of compaction, numerical simulations of a split Hopkinson test with different evolutions of the porosity were performed. Fig. 3 shows the different hydrostatic stress versus volumetric variation curves for the evolution of the porosity which were chosen for the computations.

In these simulations the input and output bars are not represented in the finite element model. Only the concrete specimen is described with special boundary conditions which account for wave transmission and

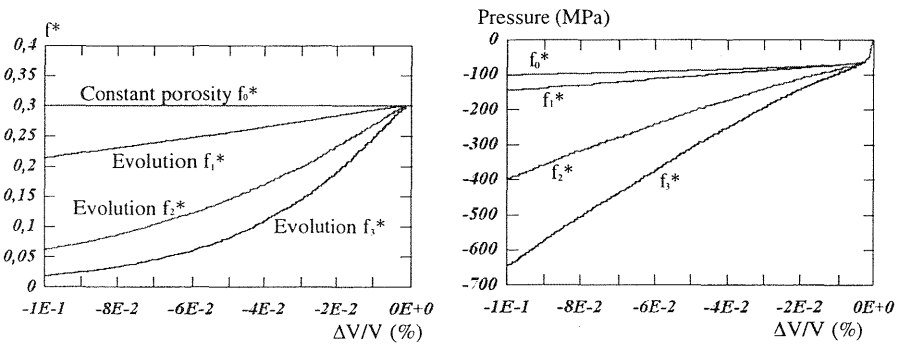

Fig. 3. Porosity vs. volumetric strain and pressure vs. volumetric strain.

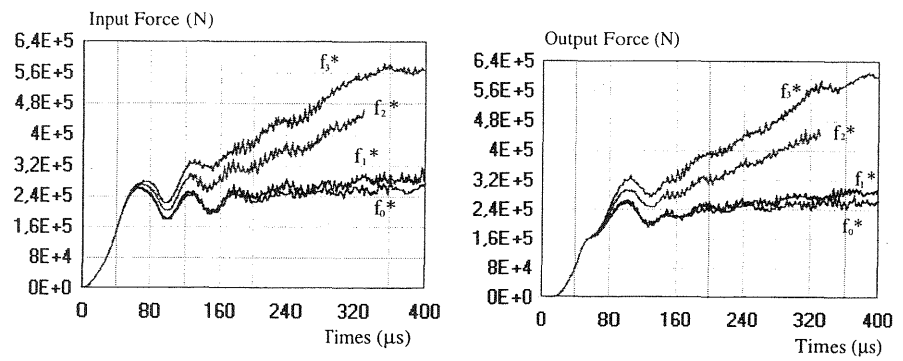

Fig. 4. Input and output forces for different porosity evolutions.

reflection. In the simulations, the input and output experimental velocities are prescribed to the confined concrete specimen and numerical results of the input and output forces are compared in Fig. 4. Axial velocities at the boundaries are prescribed by mean of rigid surfaces. These boundary conditions have in fact little influence on the computed forces (Gatuingt 1997). Radial boundary conditions are unknown in the experiment and, in the simulation, the external radial displacements of the specimen (steel jacket) are free. The computed forces increase when the porosity of the material decreases. Hence the transmitted forces which might produce cracking in a structure are expected to increase with this model compared to situations where compaction is neglected

In order to better show the influence of compaction, an impact problem is presented with two different material models for the slab. Figure 5 shows the mesh used for the simulation. Displacements are prevented on the external surface of the mesh. The impactor has a short length in order to produce a short impulsion in the slab.

The velocity of the impactor is 500 m/s which produces a stress which is sufficient to induce compaction. Figure 6 shows the velocity versus time evolution for two points placed under the impactor.

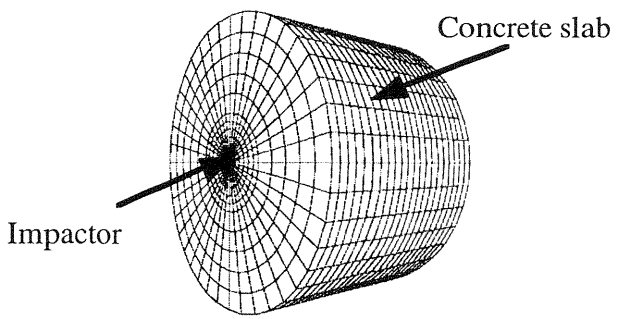

Fig. 5. 3D finite element mesh in the impact problem.

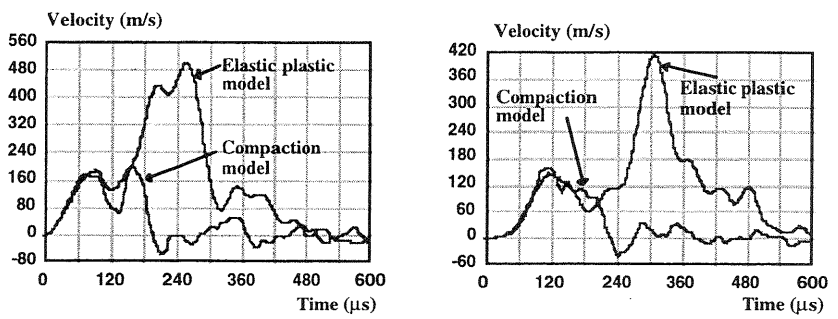

Fig. 6. Velocity evolution.

With the elastic-plastic model, we can notice that we have two very distinct waves (the elastic and the plastic one). The plastic wave for the first point has the same velocity than the impactor (there is no dissipation). For the compaction model the elastic wave is the same as for the elastic plastic model, but the second wave is faster than the plastic wave and the amplitude of this wave is lower (the dissipation is more important in this case). This computation shows that compaction has a significant influence on wave transmission. It might possibly influence spalling, or the output speed of the impactor in case of perforation of the slab which is quite often overestimated with plasticity models.

5 Conclusion

A damage plasticity model has been presented. For the sake of simplicity and computational efficiency, an explicit time integration of the constitutive relations was used for the implementation.

The chosen dynamic tests in which the concrete specimen is not submitted to extensions but essentially to plasticity in compression shows that the presented model gives correct trends.

6 References

Burlion, N. (1997) Compaction des bétons: Eléments de modélisation et caractérisation expérimentale thèse de Doctorat de l'ENS de Cachan, Cachan, France.

Cowin, S.C. & Nunziato, J.W.(1983) Linear elastic materials with voids, **J. of Elasticity**, 13, 125-147.

de Borst, R., Sluys, L.J., Muhlhaus, H.B. & Pamin, J. (1993) Fundamental Issues in Finite Element Analyses of Localization of Deformation, **Engrg. Comput.**, 10, 99-121.

Gatuingt, F. Daudeville, L. (1997) Numerical simulation of split Hopkinson tests, First European LS-DYNA3D users conference, Stratford England

Gurson, A.L. (1977) Continuum theory of ductile rupture by void nucleation and growth: Part I - Yield criteria and flow rules for porous ductile media, **Eng. Mat. and Tech.**, 99, 2-15.

Hallquist, J.O. (1995) DYNA3D: Theoretical Manual, Livermore Software Technology Corporation, Livermore USA

Mazars, J. (1986) A description of micro and macro scale damage of concrete structures, **Engrg. Fract. Mech.** 25, 729-737.

Needleman, A. Tvergaard, V. (1984) An analysis of ductile rupture in notched bars. **J. Mech. Phys. Solids.**, 32, 461-490.

Whirley, R.G. & Hallquist, J.O. (1991) DYNA3D: A Nonlinear Explicit Three-Dimensional Finite Element Code for Solid and Structural Mechanics, *User Manual*, Report UCRL-MA-10254, Lawrence Livermore National Laboratory, Livermore USA.